3D Channel Knowledge Map Construction for Cellular UAVs Based on Environmental Features

Peng Gu, Enzhi Zhou, *Member, IEEE,* Zhi Zheng, *Member, IEEE,* Zhicheng Dong, *Member, IEEE,* Ping Lan

***Abstract*—Cellular-connected unmanned aerial vehicle (UAV) communication faces challenges such as rapidly time-varying channels, dynamic blockages, and Doppler effects in low-altitude applications. Accurate and rapid channel prediction is crucial for ensuring communication reliability. As a potential technology that can enhance communication performance, channel knowledge maps (CKM) can provide channel status information (CSI) at specific locations for UAV wireless communications. However, traditional construction schemes based on measurements, ray tracing (RT), or historical CSI often fail to adequately consider the impact of environmental features (such as building layout and height), and still exhibit significant limitations in constructing three-dimensional (3D) CKMs for low-altitude urban environments with dense buildings. In this paper, we propose a deep learning network architecture named MPANet, which effectively addresses the challenge of 3D spatial CKM construction. The model not only integrates complex environmental features from height-preserving 2D images but also utilizes dual attention mechanisms to focus on key regions across both channel and spatial dimensions. This enables joint multi-altitude path loss prediction in low-altitude environments and generates 3D path loss distributions based on environmental characteristics, offering a novel solution for constructing CKMs for cellular-connected UAVs. Results demonstrate that our proposed method delivers high-precision signal path loss prediction for UAV communications. MPANet achieves a root mean square error (RMSE) below 0.2 dB across all test scenarios, exhibiting superior performance compared to traditional construction approaches.**

***Index Terms*—UAV cellular communication, channel knowledge map, path loss prediction, deep learning.**

I. Introduction

LOW-altitude small unmanned aerial vehicles (UAVs), with their high maneuverability and low cost, demonstrate significant potential in civil and commercial sectors. They are widely applied in scenarios such as traffic control, logistics transportation, emergency search and rescue, and intelligent security systems [1]. The successful execution of these critical missions heavily relies on highly reliable, low-latency beyond visual line of sight (BVLOS) communication capabilities. Cellular networks, with their extensive coverage, high capacity, mobility support, and management convenience, are regarded as the most promising communication infrastructure for supporting large-scale UAV applications. However, seamlessly extending traditional cellular networks—primarily designed for terrestrial users—into low-altitude airspace presents severe challenges. In complex urban low-altitude environments, the high-mobility three-dimensional (3D) movement of UAVs causes wireless channel characteristics, particularly path loss (PL), to fluctuate drastically and become difficult to predict with spatial location variations. This significantly impacts network coverage, link reliability, and communication efficiency.

Reliable UAV communications are highly dependent on accurate perception of wireless channel characteristics. Traditional measurement methods based on reference signals struggle in scenarios with high-speed UAV mobility and complex terrain: due to rapid channel variations, measurement results suffer from delayed updates and are susceptible to multipath interference, failing to provide stable channel state inputs for real-time tasks such as path planning, aerial photography, and target tracking [2] [3]. Path loss exhibits a strong correlation with channel quality, serving as a core parameter characterising the macro-average power attenuation of signals during propagation. Channel prediction models focusing on path loss represent a critical breakthrough for ensuring communication quality, enhancing flight safety, and optimizing resource allocation. Therefore, accurate construction of the 3D spatial path loss distribution in low-altitude environments is regarded as a key enabling technology for guaranteeing communication quality and enabling efficient operation of cellular-connected UAV networks.

To address the aforementioned challenges, channel knowledge map (CKM) have emerged as a feasible solution to meet the urgent demand for real-time and reliable channel state information (CSI) in UAV missions [4]. Based on digital twin technology, CKM transforms physical channel characteristics into computable, predictable spatio-temporal databases [5]. Through pre-computed or continuously updated learning of environmental information, it provides various location-dependent channel data (such as channel gain, path loss, signal-to-noise ratio, and signal-to-interference-plus-noise ratio). By utilizing pre-constructed channel knowledge through environmental sensing, mobile terminals can infer channel states directly based on their positional information without relying on real-time measurements that are susceptible to interference. Furthermore, theoretical research on the construction and utilization of CKM has been extensively conducted [6] [7] [8] [9]. Exploiting the spatial characteristics of CKM channels can yield performance enhancements across multiple domains. For instance, Reference [10] proposed extracting dominant path angle information from CKM and dynamically adjusting the phase of reconfigurable intelligent surface (RIS) reflection elements using location tags, thereby optimizing reflected beam alignment and enhancing signal quality. The CKMs constructed via IMNet [11] can be employed to achieve interference suppression in air-to-ground channels with non-cooperative interfering nodes. Reference [12] investigated the use of CKM for predicting Line-of-Sight (LOS) conditions, detecting dynamic scatterers (such as moving vehicles and pedestrians) by analyzing discrepancies between real-time channel responses and predicted values, thereby supporting in-

terference avoidance and trajectory tracking. To accommodate diverse application requirements, the CKM has spawned multiple variants. For instance: the channel matrix map (CMM) [13] stores the spatial distribution of multi-input multi-output (MIMO) channel matrices to directly infer channel states; the beam index map (BIM) [14] maps positional tags to optimal transmit-receive beam pairs to support low-overhead beam selection; the channel path map (CPM) which records multipath signal path characteristics [15]; and the channel gain map (CGM) which provides the spatial distribution of large-scale fading [16], amongst others. By storing channel characteristics across different dimensions, these CKM variants collectively construct a multidimensional knowledge framework for wireless transmission.

Among diverse types of CKMs, those constructed based on path loss can significantly enhance the reliability of channel modeling in obstructed areas (such as building clusters or vegetation-covered regions). Particularly in complex low-altitude terrain scenarios, path loss serves as a key physical parameter dominating large-scale fading and directly determines the CKM's capability to reconstruct the spatial distribution of channel gain. Traditional approaches to path loss prediction primarily rely on distance-based statistical models [17] [18] [19]. However, in urban low-altitude scenarios featuring buildings of varying heights and dense street greenery, such models often struggle to accurately capture complex propagation effects, resulting in significant discrepancies between predictions and actual measurements. Empirical models, meanwhile, struggle to balance prediction accuracy with computational efficiency, particularly failing to meet the real-time prediction demands of multi-altitude, dynamically changing low-altitude UAV communication scenarios. Methods for constructing comprehensive CKMs from channel data can be broadly categorized into interpolation-based and machine learning-based approaches. Interpolation-based methods directly utilise channel information from adjacent sampling locations to calculate channel information at target locations, including inverse distance weighting (IDW) [20], k-nearest neighbours (KNN) [21], and Kriging [22] [23]. These methods typically require a large number of samples for accurate map construction, which demands substantial storage capacity. Furthermore, such purely data-driven approaches often neglect established channel models. In contrast, machine learning-based methods can capture the mapping relationship from arbitrary locations to their corresponding channel information by leveraging existing channel knowledge, such as free-space path loss models and shadowing residual models. Research demonstrates that data-driven machine learning methods [24] [25] can significantly outperform empirical models and computationally intensive ray tracing (RT) algorithms in path loss prediction tasks, achieving both high accuracy and efficiency. Neural networks, as a crucial branch of machine learning, simulate the processing mechanisms of biological neurons to learn complex mapping relationships from training data, providing an effective tool for modeling channel characteristics in practical environments [26].

In recent years, significant progress has been made in deep learning-based coverage prediction and CKM modeling research [27] [28]. Models such as RadioUNet [29] and FadeNet [30] aim to predict path gain, received power, or coverage for transmitter-receiver (TX-RX) pairs in a given area by inputting building maps. The UNet learning framework utilises boundary vectors and maps as input [31], while [32] PPNet converts information related to outdoor propagation environments into path loss heatmaps. The building map models input to PMNet [33] [34] lack height information. These models are designed for large-scale channel prediction in 2D space and cannot meet the demands of 3D prediction. In [35], a U-Net enhanced with EfficientNet as its backbone explores the challenges and solutions for predicting radio coverage in complex indoor environments for millimeter-wave communications. However, 3D millimetre-wave coverage prediction in outdoor low-altitude dense building environments still faces challenges such as severe environmental obstructions and complex multipath effects. Existing models struggle to effectively capture the correlation between reflectors, scatterers, and signal propagation in complex environments, making it difficult to accurately predict 3D spatial path loss.

In response to the aforementioned challenges, this paper proposes a deep learning-based approach for constructing 3D CKM for cellular-connected UAVs. The main contributions of this work are as follows:

- Utilising the RT simulation tool Wireless InSite[32], we constructed three channel measurement datasets for low-altitude environments with dense buildings. These datasets reflect distinct scenario characteristics within the same environment, encompassing varying map scales, building height information, and TX configurations. They capture the diverse features of complex low-altitude scenarios, providing high-quality, multi-dimensional benchmark data for model training and performance evaluation.
- A construction scheme for CKM has been proposed, alongside the design of MPANet—a multi-input multi-output neural network architecture integrating environmental features with attention mechanisms. By leveraging multi-channel convolutions, it efficiently outputs multi-height channel prediction maps, enabling the construction of 3D CKMs in complex low-altitude scenarios.
- The effectiveness of the proposed MPANet model was evaluated through simulation on constructed datasets. Performance comparisons against empirical models and traditional machine learning algorithms demonstrated that MPANet achieves root mean square errors (RMSE) at the 0.1 dB level across varying heights on different scenarios, outperforming conventional prediction approaches.

This study systematically explores the modelling of low-altitude wireless channels, organised as follows:Section II establishes the system model and formally defines the channel prediction problem; Section III constructs a low-altitude channel dataset featuring diverse scenario characteristics; Section IV proposes MPANet, a deep learning network model for constructing 3D CKMs for cellular-connected UAVs in low-altitude environments; Section V presents experimental results of MPANet across different scenarios; Section VI summarises the research findings and outlines future research directions.

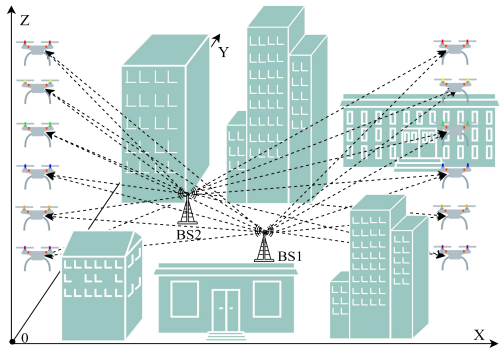

Fig. 1. Illustration of the cellular-connected UAV system.

II. System Modeling and Problem Formulation

We consider the cellular-connected UAV system depicted in Fig. 1, in which the cellular connected UAV is served by its associated base station (BS) in the same frequency band, and any UAV can communicate with BS. It is assumed that the flight altitude of these UAVs is between $H_{\min}$ and $H_{\max}$, and BS is near the ground or at low altitude, where $H_{\min}$ and $H_{\max}$ are the minimum and maximum flight altitude of UAVs. We consider a 3D region $X \times Y \times Z$, where X, Y and Z represent the length, width, and height of the entire spatial domain. The operational spatial domain for the UAVs is defined as $\mathbf{S} = \{(x, y, z) \,|0 \leq x \leq X, 0 \leq y \leq Y, H_{\min} \leq \mathrm{z} \leq H_{\max}\}$.

We perform sparse sampling in the spatial domain $\mathbf{S}$ to obtain discrete spatial coordinates. The CKM channel knowledge matrix corresponding to these discrete spatial coordinates is defined as $\mathbf{C}$, where $c_{i,j,k}$ denotes the channel data at the corresponding spatial location for the element in the channel knowledge matrix $\mathbf{C}$ indexed by i, j, k.

$$c_{i,j,k} = \begin{cases} 0, & \text{Otherwise} \\ P_{i,j,k}, & 1 \leq i \leq N_x,\ 1 \leq j \leq N_y,\ 1 \leq k \leq N_z \end{cases}, \tag{1}$$

where$P_{i,j,k}$ denotes the ground-truth path loss, N_x, N_y and N_z represent the sample sizes in each dimension respectively, and the dimension size of $\mathbf{C}$ is $N_x \times N_y \times N_z$.

The core objective of this paper is to establish an efficient and accurate predictive function, enabling rapid and precise mapping from environmental features at three-dimensional locations to PL values. This addresses the computational efficiency bottleneck encountered in traditional electromagnetic simulations within multi-height scenarios. The overall construction plan of the CKM can be represented as follows:

$$\arg\min_{f_\theta} \sum_{\omega} |f_\theta(\mathbf{E}, \omega) - P_\omega|. \tag{2}$$

That is, finding the optimal prediction function to minimize the overall error between the predicted and actual values, and outputting the predicted path loss value of the location by inputting the environmental feature at the spatial location. $|\cdot|$ is the absolute value calculation, $f_\theta(\mathbf{E}, \omega)$ is the mapping function of path loss, where $\mathbf{E}$ is the environmental characteristic matrix such as building layout and height, ω is the position coordinate (i, j, k), i, j, k are integers, and f_θ is the parametric prediction model.

A data-driven approach can be employed to construct the CKM, with the core workflow illustrated in Fig. 2. CSI is first obtained through UAV field measurements or high-fidelity channel simulations. After data preprocessing, a dataset is constructed using environmental features $\mathbf{E}$ and location coordinates ω as inputs, with path loss as the label. This dataset trains a deep learning network that takes multi-channel building environmental parameters as input. The network learns the mapping relationship from complex environmental features to spatial channel characteristics and undergoes continuous optimization during training, ultimately yielding an optimal model with strong generalization capabilities. Through fine-tuning techniques, the pre-trained model can be adapted using limited data from cross-scenario applications to efficiently infer the 3D path loss distribution in new environments, thereby generating high-precision CKMs. By training on large-scale, diverse scenario data, the model captures universal channel propagation patterns, enabling stable cross-scenario prediction performance.

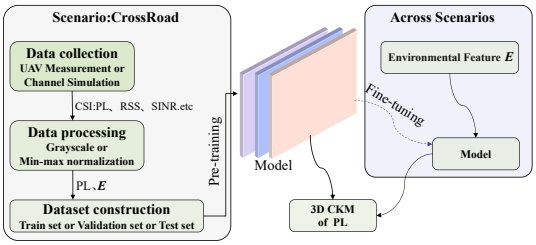

Fig. 2. Overview of CKM construction scheme.

III. Dataset Generation

This section presents the CrossRoad Map, a simulated dense urban environment map we created. Additionally, we discuss the configuration of three different scenarios and detail the preparation of the path loss dataset constructed for training and validation of the proposed model.

A. Simulation Environment Configuration

RT can can predict multi-dimensional channel information in both indoor and outdoor wireless environments, such as received signal strength, signal-to-interference-plus-noise ratio (SINR), propagation delay, and angular distributions. By solving physical optics equations for electromagnetic wave propagation, this technique simultaneously analyzes the impact mechanisms of environmental complexity (e.g., building layouts, material properties) and equipment parameters (e.g., transceiver power, antenna gain) on path loss. Its outputs support BS deployment planning, system optimisation, and user equipment (UE) multi-channel management tasks. The commercial RT tool Wireless InSite is widely adopted due to its low-error measurement accuracy and user-friendly interface, which we utilize for 3D scenario modeling and channel characterization. It should be noted that this study focuses on low-altitude UAV communication scenarios in densely

built urban crossroads areas, with particular emphasis on the propagation characteristics between base stations and low-altitude terminals.

Specifically, we constructed a densely built environment at an intersection. The map dimensions were set at 500m×500m, with two main thoroughfares running through it. Green belts are set on both sides of the street, and sidewalks are set next to the green belts. Along one side of the pavements stood densely packed buildings of varying heights, ranging from 50m to 150m, to closely replicate the urban landscape of the real world. The map modeling is shown in Fig.3.

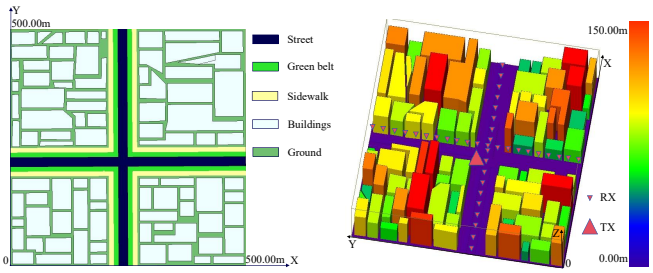

(a) CrossRoad Plan. (b) 3D Map.

Fig. 3. Map in RT simulation.

In Wireless InSite, we achieve the recreation of densely built-up urban environments by combining various scene features such as terrain, cityscapes, floorplans, foliage coverage, and unspecified objects. To ensure the accuracy of electromagnetic parameters, all scene elements require the configuration of corresponding material properties (dielectric constant, conductivity, etc.). We have assigned diverse material properties to each component of the map modelling. See Table I for details.

TABLE I
ENVIRONMENT CONFIGURATION PARAMETERS

Scenario	Material	Dielectric constant	Conductivity
Street	Asphalt	5.72	0.0005
Sidewalk	Brick	4.44	0.001
Buildings	Concrete	7	0.015
Ground	Wet Earth	20	0.02

Within the altitude range covering the majority of low-altitude terminal operations, the minimum and maximum altitudes are designated as $H_{\min} = 50\text{m}$ and $H_{\max} = 50\text{m}$, respectively. RXs are deployed uniformly spaced at 1m intervals, with $N_x = N_y = 500$. The TX adopts a half wave dipole antenna, which is placed at the height of 2m and 25m respectively, and its carrier frequency is set at 6GHz. Both TX and RX antennas utilise vertical polarisation. During RT simulation, each ray is configured to undergo a maximum of 6 reflections, 2 transmissions, and 1 diffraction.

B. Constructed Dataset

In practical applications, to ensure model accuracy while reducing the cost of UAV-collected path loss data, we adopt a layered altitude sampling strategy with 10m intervals, while maintaining the same planar sampling resolution. This approach reduces data acquisition costs by 88% compared to the 1m altitude interval strategy. Furthermore, to validate the generalization capability of the trained model, we utilize data from other scenarios for evaluation. The study employs the following data processing methods: raw numerical data obtained from RT simulations undergoes min-max normalization for grayscale preprocessing to generate accurate path loss distribution maps. To further expand the sample size, various data augmentation techniques are employed to create additional samples, thereby establishing an image vision feature-based dataset.

Through varied environmental configurations, we constructed three datasets bearing the same names as the scenarios (see Table II). In CrossRoad_air1 and CrossRoad_ground, we set TX at the low altitude and near ground positions of the map center, and the map size remains unchanged. In CrossRoad_air2, we altered the map dimensions and placed the TX at low altitude near the center point. By adjusting both the map scale and TX location, we simulated the diverse requirements encountered in practical deployments.

The sample points in the dataset can be represented as triples: $(\mathbf{M}, \mathbf{T}, \bar{\mathbf{P}})$. Here, $\mathbf{M}$ denotes the geographical map, $\mathbf{T}$ represents the TX location map, and $\bar{\mathbf{P}}$ signifies the processed PL map, each with a dimensionality of 256×256.

Pre-processing. The original map is converted into a binary representation of built environments and open spaces through binarisation, where built environments are assigned a value of 1 and open spaces are assigned a value of 0. Subsequently, building heights ranging from 0m to 150m are linearly mapped to grey values between 1 and 255, with the mapped grey values then assigned to the built environments. This process preserves elevation information within the two-dimensional planar image, providing spatial structural features for subsequent analysis.

$$\mathbf{M}_{i,j} = \begin{cases} 0, & \text{Otherwise} \\ 1 + 254 \cdot \dfrac{h_{i,j} - h_{\min}}{h_{\max} - h_{\min}}, & \text{Building Area} \end{cases}, \tag{3}$$

where $h_{i,j}$ is the height value of the building at this location, $h_{\min}$ and $h_{\max}$ are the shortest and highest values of the building in the map respectively, and Building Area is used to distinguish built environments from free space.

$$\mathbf{T}_{i,j} = \begin{cases} 0, & \text{Otherwise} \\ 255, & (i,j) = L_{\text{TX}} \end{cases}. \tag{4}$$

Here, $L_{TX} = (x_{tx}, y_{tx})$ denotes the position of TX on the map. Minimum-maximum normalised greyscale processing is employed to map path loss values (in dB) to a greyscale range of 0–255, with a minimum of 0 dBm and a maximum of 255 dBm. The fixed step size of 1 dBm is adopted because the fine step size will not have a significant impact on the prediction performance. For each altitude level (corresponding to sampling altitude level $N_z = 6$), there are:

$$\bar{\mathbf{P}}_{i,j,k} = 255 \cdot \frac{P_{i,j,k} - P_{\min}}{P_{\max} - P_{\min}}. \tag{5}$$

$P_{i,j,k}$ is the path loss value of position (i,j) at altitude level k, while $P_{\min}$ and $P_{\max}$ represent the minimum and maximum values of the sampled path loss. Fig. 4 illustrates the path

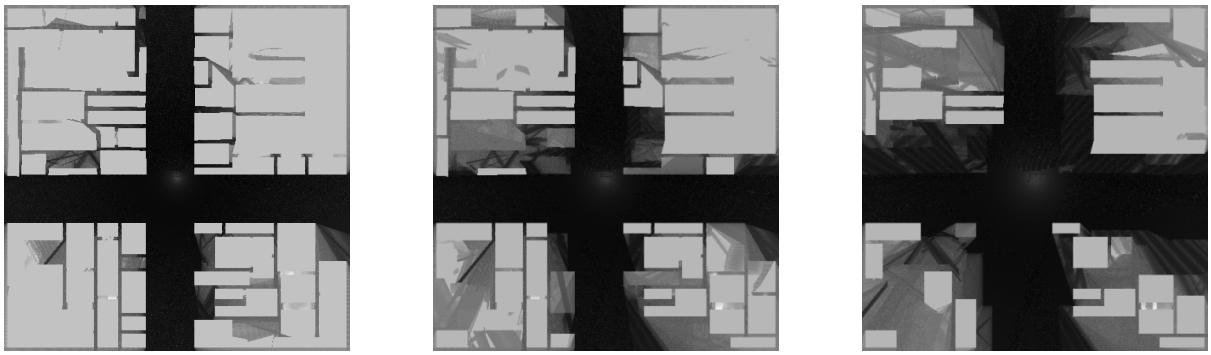

(a) k = 2,z = 60m. (b) k = 4,z = 80m. (c) k = 6,z = 100m.

Fig. 4. Min-max normalized grayscale path loss images at three different altitudes in CrossRoad_air1.

loss distribution across three altitudes in the CrossRoad_air1 scenario, where lighter shades indicate higher path loss values. The path loss distribution correlates with building height and surrounding environmental features. As building layouts vary at different altitudes, the resulting path loss distributions consequently differ.

Data augmentation. Generally speaking, expanding the dataset size can effectively enhance the training efficacy of deep learning network architectures, meaning that larger datasets typically yield superior model performance. Here, we employ two data augmentation methods—cropping and rotation—to increase the dataset size. The original environmental map and TX images measure 500×500 pixels, with each pixel containing height information. Using the map centre as an anchor point, a sliding window strategy is employed to crop 256×256 sub-images at fixed intervals. Simultaneously, identical operations are performed on path loss maps at varying elevations to ensure data consistency. Rotational transformations at different angles are then applied to the cropped sub-images, further enriching data diversity.

Through the above data processing, we constructed a larger dataset encompassing diverse network configurations and environmental characteristics (see Table II for details). This strategy effectively enhanced the model's generalisation capability while preserving the spatial structure and physical significance of the original data.

TABLE II
PARAMETERS OF DATASET

Dataset	Frequency (GHz)	TX Location (m)	Map Size (m)	Total of Data
CrossRoad_ air1	6	(250,250,25)	500×500	9604
CrossRoad_ ground	6	(250,250,2)	500×500	2401
CrossRoad_ air2	6	(200,200,25)	450×450	1521

IV. THE MULTI-HEIGHT PATHLOSS ATTENTION NETWORK: MPANET

We propose a multi-altitude path loss prediction model specifically designed for dense urban low-altitude environments. The core concept involves effectively integrating environmental geometric features with transmitter location information, and achieving joint accurate prediction of multi-altitude path loss through multi-scale feature extraction and attention mechanisms, ultimately enabling the construction of 3D CKMs. This section will elaborate on the proposed deep learning network architecture and detail the training process.

A. Overall Network Architecture

The proposed MPANet in this study is a deep learning architecture designed for complex low-altitude wireless propagation environments. Its core lies in adopting an encoder (16× downsampling)-decoder (16× upsampling) structure, integrating skip connections, multi-scale dilated convolution modules, and dual attention mechanisms for both channels and spatial domains. The network adopts the end-to-end training mode, which can generate multi-channel path loss CKM from the input characteristics of two channels (environmental geometry information and TX position information), performing pixel-level regression prediction while maintaining 256×256 spatial resolution.

Encoder-Decoder. The encoder-decoder architecture is a widely adopted neural network framework in deep learning and across domains such as natural language processing (NLP), computer vision (CV), and other fields. It is particularly well-suited for tasks like path loss prediction that require dense prediction from input to output.

The encoder is responsible for extracting high-level semantic features through multi-stage convolutional and pooling operations, progressively compressing the input into a low-dimensional feature representation. The encoder in MPANet consists of four downsampling stages, each containing convolutional layers, normalization, ReLU activation, and downsampling operations, ultimately producing a low-resolution, high-channel-count feature representation. Its shallow features capture fine geometric structures such as building edges and street layouts; mid-level features adequately identify building clusters and green belts; while deep features comprehend large-scale spatial contexts such as global layout and terrain trends, enabling the model to understand the overall propagation environment. The decoder is responsible for progressively upsampling the feature maps from the encoder back

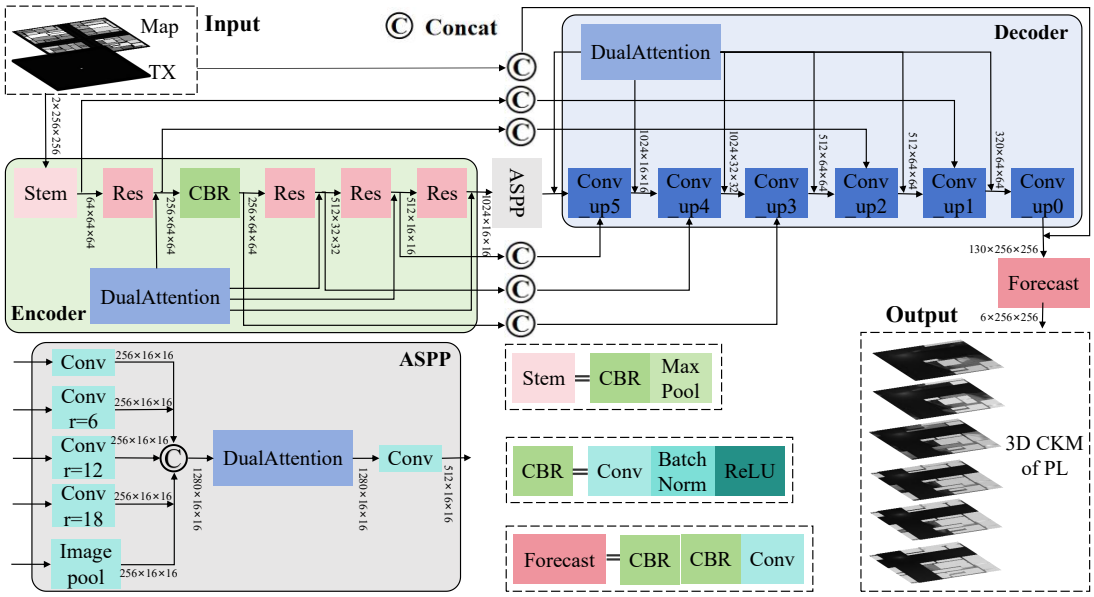

Fig. 5. The proposed network framework of MPANet.

to the original resolution and generating multi-altitude path loss predictions. It comprises three main upsampling stages, each consisting of upsampling operations, concatenation with skip-connected features from corresponding encoder stages, convolutional operations, and ReLU activation. Finally, the prediction head outputs the 3D CKM of path loss.

Skip connection. It refer to a technique widely used in deep neural networks where the inputs from earlier layers are directly combined with the outputs of later layers. This approach enables direct information flow across different network levels, effectively mitigating the gradient vanishing problem in deep architectures. In MPANet, while the encoder progressively reduces spatial resolution through pooling operations and the decoder performs step-wise upsampling via deconvolution, the spatial information and edge details from the original input image undergo gradual reconstruction, ultimately transforming low-resolution feature maps into pixel-wise segmentation results. To further compensate for the information loss during encoder downsampling, we introduce concatenation layers that directly link feature maps from the encoder stages to corresponding decoder stages. This skip connection mechanism performs feature fusion along the channel dimension, allowing the decoder to access high-resolution spatial details from corresponding encoder locations during upsampling. This architectural design ensures critical propagation-related features—such as building edges and small obstacles—are accurately processed, significantly enhancing both the precision and spatial localization accuracy of path loss predictions.

Atrous Spatial Pyramid Pooling(ASPP). Dilated convolution is a specialized convolutional operation that introduces gaps between kernel elements, enabling the capture of multi-scale contextual information without significant resolution reduction. ASPP leverages this advantage by employing multiple parallel branches with different dilation rates ($r = 6, 12, 18$), performing parallel dilated convolutional sampling at varying rates. Additionally, ASPP incorporates a standard convolutional branch and an image pooling branch to capture original-scale features and image-level global contextual information respectively. These sampling results are subsequently concatenated and processed through a convolution layer to reduce channel dimensions to the target number. This operational scheme effectively captures environmental features at multiple scales, significantly enhancing MPANet's comprehension capability for diverse environmental characteristics.

Dual Attention Module(DualAttention). The attention mechanism is a technique that enables models to focus on critical information while ignoring irrelevant details during processing, effectively enhancing both processing efficiency and accuracy. The DualAttention integrated by MPANet is composed of channel attention (CA) and spatial attention (SA), which are connected in serial mode.

CA aims to capture the relative importance of different feature channels. By assigning varying weights to channels, it enhances significant channel features while suppressing less relevant ones. In MPANet, this is implemented through global average pooling followed by convolutional layers and activation functions to generate channel weights, which are then multiplied channel-wise with the original input features. This mechanism enables the model to learn which feature channels are more crucial for the path loss prediction task. SA allows the model to adaptively learn attention weights for different spatial regions. First, max pooling and average pooling are applied along the channel dimension to the feature maps refined by channel attention. The resulting two feature maps are concatenated and processed through convolutional operations, followed by an activation function to generate a spatial weight map. This map is then multiplied element-wise with the input features. This mechanism directs the network's focus to regions particularly relevant for path loss prediction,

such as areas near TX antennas and building edges.

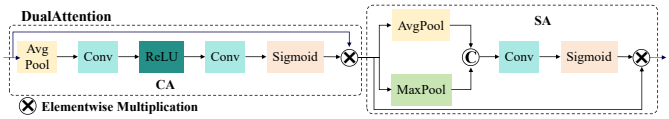

Fig. 6. DualAttention architecture.

Embedded within both the encoder-decoder structure and the ASPP module, this DualAttention adaptively recalibrates feature maps, ensuring the network concentrates on the most critical information across different levels and scales.

Forecast. The forecast head comprises three convolutional layers, ultimately mapping the channel count from 130 to 6. This corresponds to path loss values at multiple different heights, thereby enabling CKM construction.

B. Model Training

We implemented the MPANet model using the PyTorch framework with computational acceleration provided by an NVIDIA GeForce RTX 4090 GPU. The training process employed the Adaptive Moment Estimation (Adam) optimizer, which computes first and second moment estimates of gradients to provide adaptive learning rates for each parameter, thereby promoting faster and more stable convergence during training. The initial learning rate was set to $1e^{-4}$ with a step decay strategy, multiplying the learning rate by 0.5 every 20 training epochs. The batch size was fixed at 32, balancing memory utilization efficiency and training stability. Input data was normalized to the [0, 1] range through scaling, and each dataset was split into training and testing sets with a 9:1 ratio. These procedures significantly enhanced training stability.

MPANet utilizes multi-altitude mean squared error (MSE) as its loss function. Specifically, the model simultaneously predicts path loss distributions across multiple altitude layers, computes the MSE between predicted and ground-truth values at each altitude, and sums the MSE across all altitudes as the final loss. This design enables the model to optimize prediction performance across all altitude layers concurrently rather than processing each height independently. At the conclusion of each training epoch, model performance was evaluated on the validation set, assessing not only global performance metrics but also prediction accuracy at individual altitude layers.

V. Experiments and Analysis

This section presents statistical and visual results obtained in both the CrossRoad scenario and across scenarios to validate the applicability and effectiveness of MPANet.

A. CKM Construction

Root Mean Square Error (RMSE). A commonly used loss function in regression analysis that calculates the overall difference between predicted values and actual values , thereby quantifying the model's overall accuracy. The formula is as follows:

$$RMSE\left(\hat{P},P\right)=\sqrt{\frac{1}{N}\sum_{n=1}^{N}\left(\hat{P}_n-P_n\right)^2}, \tag{6}$$

where N denotes the number of sampling points, $\hat{P}_n \in \hat{P}$ and $P_n \in P$ represent the predicted and actual PL values at the nth sampling point, respectively.

Mean Absolute Error (MAE). Refers to the average value of the absolute difference between the predicted value and the real value of the model.

$$MAE\left(\hat{P},P\right)=\frac{1}{N}\sum_{n=1}^{N}\left|\hat{P}_n-P_n\right|. \tag{7}$$

Mean Absolute Percentage Error (MAPE). Commonly used to measure prediction accuracy, it represents the average percentage error between the predicted value and the actual value relative to the actual value. A smaller value indicates a better model. The formula is as follows:

$$MAPE\left(\hat{P},P\right)=\frac{1}{N}\sum_{n=1}^{N}\left|\frac{\hat{P}_n-P_n}{P_n}\right|\times 100\%. \tag{8}$$

The model was evaluated under different environmental configurations as described in Table II. Table III presents the RMSE and MAE values of the MPANet model across three scenarios. The overall test error remains below 0.03 dB in all scenarios, confirming the effectiveness and reliability of the proposed model through its performance in training, validation, and testing phases. The MAPE values for each dataset at different heights are shown in Table IV. The results indicate that although MPANet exhibits varying prediction performance across different heights, it still demonstrates overall robust channel modeling capabilities for path loss. In the CrossRoad_ground dataset, the MAPE values across all altitude layers are generally higher than in other datasets. This can be attributed to the most complex propagation conditions when the BS is positioned near the ground level, where signal reflection, diffraction, and scattering effects are more pronounced, thereby increasing prediction difficulty. MPANet's prediction performance does not exhibit a monotonic variation with altitude but rather shows fluctuations across different heights. At certain altitudes, the model performance may degrade due to varying building distributions. Overall, the proposed model effectively captures the impact of building layouts and terrain on signal propagation in low-altitude environments, achieving satisfactory prediction performance across different datasets and altitude layers.

TABLE III
Performance Analysis Across Scenarios in CrossRoad

Scenario	Training Error		Validation Error		Testing Error	
	RMSE	MAE	RMSE	MAE	RMSE	MAE
CrossRoad_air1	0.02197	0.01385	0.02541	0.01532	0.02511	0.01504
CrossRoad_ground	0.01984	0.01275	0.02491	0.01632	0.02488	0.01621
CrossRoad_air2	0.01947	0.01256	0.02564	0.01706	0.02189	0.01397

Given the availability of labeled data, path loss prediction can be formulated as a supervised learning problem of the regression type. For path loss observations and corresponding input features (such as antenna separation distance, operating frequency, distance, etc.), various machine learning algorithms

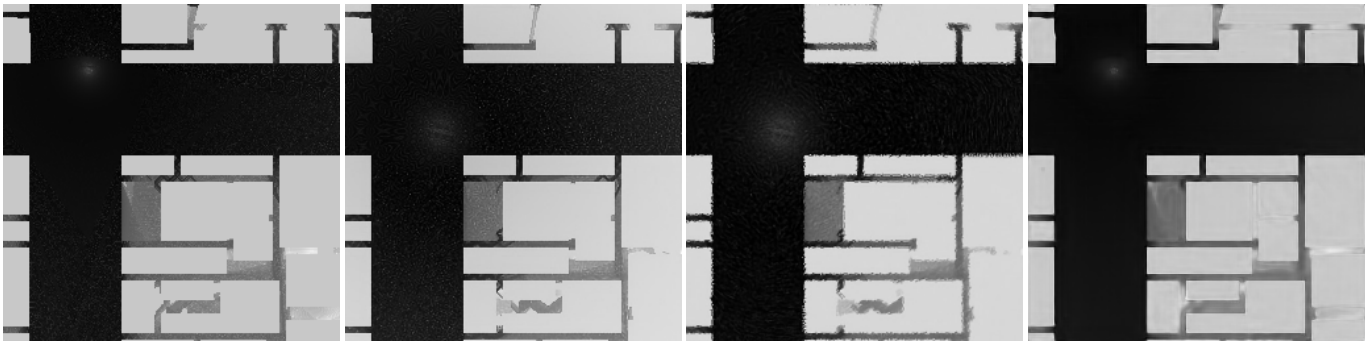

(a) z=50m Wireless InSite. (b) Prediction(mmMAGIC). (c) Prediction(KNN). (d) Prediction(MPANet).

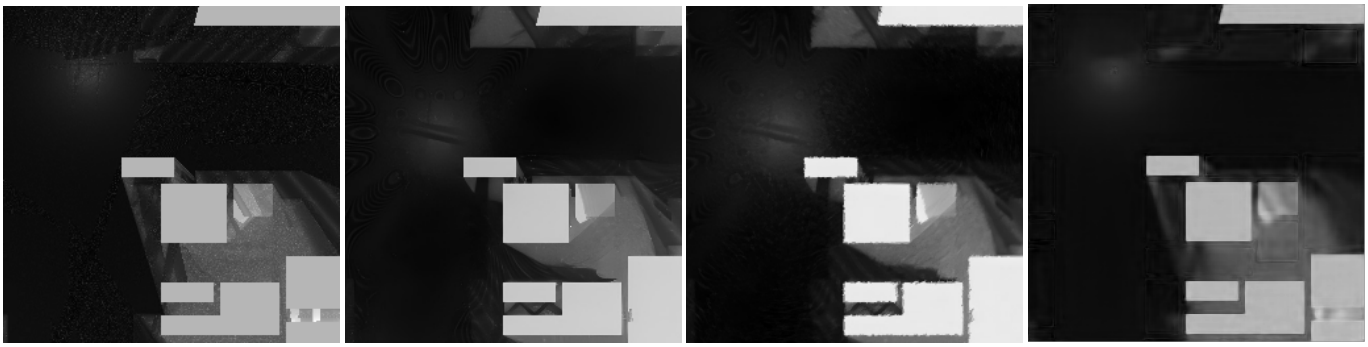

(e) z=100m Wireless InSite. (f) Prediction(mmMAGIC). (g) Prediction(KNN). (h) Prediction(MPANet).

Fig. 7. Path loss prediction maps for mmMAGIC, KNN, and MPANet at different elevation layers, where path loss values are mapped to different grayscale values. Subfigures (a), (b), (c), and (d) correspond to the altitude layer of z = 50 m, while subfigures (e), (f), (g), and (k) correspond to the altitude layer of z = 100 m.

TABLE IV
MAPE ACROSS ALTITUDE LAYERS UNDER DIFFERENT SCENARIOS IN CROSSROAD

Different heights	MAPE		
	CrossRoad_air1	CrossRoad_ground	CrossRoad_air2
k=1,z=50m	1.071%	1.864%	1.639%
k=2,z=60m	3.219%	3.646%	3.271%
k=3,z=70m	1.563%	2.604%	2.228%
k=4,z=80m	2.818%	3.331%	3.114%
k=5,z=90m	1.944%	4.192%	3.795%
k=6,z=100m	2.439%	4.710%	2.168%

or empirical models can be employed to derive robust estimation functions for path loss prediction. This enables accurate mapping from input features to output path loss values. Empirical path loss models require probabilistic modeling to determine line-of-sight (LOS) and non-line-of-sight (NLOS) conditions at specific distances. To ensure fairness in comparison, we computed path loss using LOS and NLOS conditions determined based on environmental map information.Table V presents a performance comparison among multiple machine learning algorithms, empirical models, and MPANet across different altitude layers in dense urban low-altitude environments. The performance of all compared models exhibits fluctuations with changing altitude, reflecting variations in propagation environments across different heights. Our proposed model demonstrates clear superiority over traditional regression algorithms and empirical models, achieving the lowest RMSE values across all tested altitudes, which confirms its exceptional capability for accurate path loss prediction in complex scenarios.

TABLE V
PERFORMANCE COMPARISON OF MACHINE LEARNING ALGORITHM, EMPIRICAL MODEL AND MPANET AT DIFFERENT ALTITUDES

Model	RMSE					
	z=50m	z=60m	z=70m	z=80m	z=90m	z=100m
Linear Regression	44.7674	52.2666	51.3824	48.0081	46.0038	52.5925
Decision Tree	26.3443	33.6986	29.0673	25.1161	27.2793	32.4297
K-Nearest Neighbors	7.1841	9.0964	8.7791	8.0589	7.5309	9.3974
3GPP TR 38.901 [37]	12.371	12.954	13.938	14.081	14.484	15.589
ITU-R P.1411 [38]	8.2227	8.8174	9.8841	9.8889	10.448	11.122
mmMAGIC [39]	4.7482	4.8680	7.1235	8.9455	10.212	11.421
MPANet	**0.01686**	**0.01734**	**0.01818**	**0.02042**	**0.02219**	**0.02183**

Fig.7 presents the path loss prediction maps generated by the KNN machine learning algorithm, the mmMAGIC empirical model, and the proposed MPANet model at two different altitude levels. Specifically, while the KNN algorithm emphasizes inter-data correlations and relies on limited local samples for prediction, it cannot establish a global mapping

function based on hierarchical features like deep learning networks. While the mmMAGIC method incorporates physical understanding of propagation mechanisms, its inherent model limitations prevent effective handling of complex wireless propagation phenomena such as reflection, diffraction, and scattering. Both methods exhibit significant discrepancies from ground-truth measurements in simulations. In contrast, our MPANet maintains exceptionally low and stable error levels across different altitudes, effectively capturing and learning the complex underlying propagation physics at various heights.

B. Cross-Scenario CKM Construction

To validate the generalization capability of MPANet in three-dimensional space, we constructed a new scenario similar to CrossRoad and selected 10% of the collected data for simulation experiments. As demonstrated in Table VI, our MPANet maintains exceptional performance even in this novel environment, achieving a root mean square error below 0.2 dB and outperforming both empirical models and traditional machine learning algorithms. This experiment strongly demonstrates that MPANet successfully addresses the challenge of continuous generalized prediction across 3D space for complex low-altitude channel modeling. It conclusively proves that the model genuinely learns transferable physical principles of wireless propagation, enabling it to extend its deep understanding of spatial and propagation mechanisms to new locations within 3D space, thereby accurately predicting path loss at arbitrary altitudes.

Therefore, in practical deployment scenarios, there is no longer a need for dense and expensive measurement sampling across all altitudes. By training the MPANet model, we can obtain continuous, high-accuracy path loss prediction capabilities throughout the entire 3D space. This approach significantly reduces both data acquisition costs and computational overhead, providing an efficient and reliable deep learning solution for low-altitude communication network planning and optimization.

TABLE VI
PERFORMANCE COMPARISON OF MPANET ACROSS DIFFERENT SCENARIOS

Scenarios	MAE	RMSE
CrossRoad_air1	0.02511	0.01504
CrossRoad_ground	0.01621	0.02488
CrossRoad_air_2	0.01397	0.02189
Cross-Scenario	0.08965	0.13325

VI. CONCLUSION

This work introduces a method for constructing 3D CKMs for cellular-connected UAVs based on image-based visualisation. By employing sophisticated modeling techniques to create multi-dimensional RT channel datasets and applying them to machine learning, it systematically investigates the challenges and solutions in path loss prediction for cellular-connected UAVs within complex urban low-altitude environments. The method leverages environmental features and the powerful capabilities of attention mechanisms to enhance the generalizability and effectiveness of radio coverage prediction in densely built environments. Our experiments demonstrate that MPANet overcomes the limitations of traditional path loss models in adapting to three-dimensional space, successfully achieving the construction of 3D CKMs for scenarios with dense building clusters. Particularly in typical use cases such as low-altitude UAV communications and penetration loss through high-rise buildings, the model exhibits high-precision prediction capabilities. As wireless communication expands into three-dimensional space, the proposed technical framework provides crucial support for overcoming the propagation modeling bottlenecks inherent in achieving integrated "air-space-ground-sea" ubiquitous coverage.

In summary, this research represents a significant step forward in constructing wireless coverage CKMs for low-altitude environments towards 5G or 6G systems. It provides an end-to-end channel prediction modeling toolchain to enhance connectivity for spatial-intensive built environments and low-altitude communication systems (such as UAV BSs and aerial IoT). Future work may focus on further refining these models, for instance by incorporating environmental semantic information (e.g., building usage) to develop knowledge-augmented hybrid prediction models. Alternatively, exploring propagation characteristics modeling in the Terahertz (THz) band for ultra-dense environments or integrating with RIS to develop channel optimization algorithms could be pursued. These directions will establish theoretical and technical foundations for emerging application scenarios such as smart city three-dimensional networking and space-based platform communication.

REFERENCES

[1] G. Geraci et al., "What Will the Future of UAV Cellular Communications Be? A Flight From 5G to 6G," *IEEE Commun. Surv. Tutor.*, vol. 24, no. 3, pp. 1304-1335, thirdquarter 2022.

[2] T. Wang, C. Zhang and H. Liang, "CKM-Assisted UAV Communication Design," *Proc. IEEE 99th Veh. Technol. Conf. (VTC2024-Spring)*, Singapore, 2024, pp. 1-6.

[3] C. Zhan, H. Hu, Z. Liu, J. Wang, N. Cheng and S. Mao, "Aerial Video Streaming Over 3D Cellular Networks: An Environment and Channel Knowledge Map Approach," *IEEE Trans. Wireless Commun.*, vol. 23, no. 2, pp. 1432-1446, Feb. 2024.

[4] Y. Zeng and X. Xu, "Toward environment-aware 6G communications via channel knowledge map," *IEEE Wireless Commun.*, vol. 28, no. 3, pp. 84-91, Jun. 2021.

[5] Y. Zeng et al., "A Tutorial on Environment-Aware Communications via Channel Knowledge Map for 6G," *IEEE Commun. Surv. Tutor.*, vol. 26, no. 3, pp. 1478-1519, thirdquarter 2024.

[6] Z. Dai et al., "Prototyping and Experimental Results for Environment-Aware Millimeter Wave Beam Alignment via Channel Knowledge map," *IEEE Trans. Veh. Technol.*, vol. 73, no. 11, pp. 16805-16816, Nov. 2024.

[7] Y. Li, X. Wang, Z. Zheng, J. Guo and Z. Fei, "Joint Trajectory and Transmit Power Design for Cellular-Connected UAVs Via Differentiable Channel Knowledge Map," *IEEE Trans. Veh. Technol.*, early access.

[8] Z. Dai, D. Wu, X. Xu and Y. Zeng, "Generating CKM Using Others' Data: Cross-AP CKM Inference with Deep Learning," *IEEE Trans. Veh. Technol.*, early access.

[9] X. Wang et al., "Channel Knowledge Map-Aided Channel Prediction With Measurements-Based Evaluation," *IEEE Trans. Commun.*, vol. 73, no. 5, pp. 3622-3636, May 2025.

[10] D. Ding, D. Wu, Y. Zeng, S. Jin, and R. Zhang, "Environment-aware beam selection for IRS-aided communication with channel knowledge map," *Proc. IEEE Globecom Workshops*, pp. 1-6, 2021.

[11] L. Zhao, Z. Fei, X. Wang, J. Huang, Y. Li and Y. Zhang, "IMNet: Interference-Aware Channel Knowledge Map Construction and Localization," *IEEE Wireless Commun. Lett.*, vol. 14, no. 3, pp. 856-860, Mar. 2025.

[12] S. Zeng, X. Xu, Y. Zeng, and F. Liu, "CKM-assisted LoS identification and predictive beamforming for cellular-connected UAV," *Proc. IEEE ICC*, 2023.
[13] S. J. D. Wu, Y. Zeng and R. Zhang, "Environment-aware and training-free beam alignment for mmwave massive mimo via channel knowledge map," *Proc. IEEE ICC Workshops*, pp. 1-7, 2021.
[14] Z. Dai et al., "Prototyping and Experimental Results for Environment-Aware Millimeter Wave Beam Alignment via Channel Knowledge map," *IEEE Trans. Veh. Technol.*, vol. 73, no. 11, pp. 16805-16816, Nov. 2024.
[15] S. Zeng, X. Xu, Y. Zeng, and F. Liu, "CKM-assisted LoS identification and predictive beamforming for cellular-connected UAV," *Proc. IEEE ICC*, 2023.
[16] J. Chen, R. Gao, J. Wang, S. Sun and Y. Wu, "Channel Gain Map Construction Based on Subregional Learning and Prediction," *IEEE Trans. Veh. Technol.*, vol. 74, no. 6, pp. 9852-9857, Jun. 2025.
[17] U. Etuk Uyoata, "LoRa Network Planning Using Empirical Path Loss Models," *Proc. Nigeria 4th Int. Conf. Disruptive Technol. Sustain. Develop.*, Lagos, Nigeria, 2022, pp. 1-5.
[18] M. Pinem, F. Rahma, A. H. Rambe, N. Adilah, Hendri and Y. Munthe, "Estimation of Path Loss Propagation Model on Homogeneous Vegetation for 2100 MHz Mobile Communication Networks," *Proc. 6th Int. Conf. Elect., Telecommun. Comput. Eng.*, Medan, Indonesia, 2022, pp. 106-110.
[19] P. Fuster-Parra and S. Galmés, "Wireless Propagation Modeling Through Bayesian Networks," *IEEE Access*, vol. 12, pp. 181632-181643, 2024.
[20] D. Denkovski, V. Atanasovski, L. Gavrilovska, J. Riihijarvi, and P. Mähonen, "Reliability of a radio environment map: Case of spatial interpolation techniques," *Proc. ICST Conf. Cogn. Radio Oriented Wireless Netw. Commun.*, 2012, pp. 248-253.
[21] R. Deng, Z. Jiang, S. Zhou, S. Cui and Z. Niu, "A two-step learning and interpolation method for position-based channel database construction," *Proc. IEEE Globecom*, Abu Dhabi, UAE, 2018, pp. 1-6.
[22] K. Sato and T. Fujii, "Kriging-based interference power constraint: Integrated design of the radio environment map and transmission power," *IEEE Trans. Cogn. Commun. Netw.*, vol. 3, no. 1, pp. 13-25, Mar. 2017.
[23] H. Li, P. Li, G. Cheng, J. Xu, J. Chen, and Y. Zeng, "Channel knowledge map (CKM)-assisted multi-UAV wireless network: CKM construction and UAV placement," *J. Commun. Netw.*, vol. 8, no. 3, pp. 256-270, Sep. 2023.
[24] M. Ayadi, A. B. Zineb, and S. Tabbane, "A UHF path loss model using learning machine for heterogeneous networks," *IEEE Trans. Antennas Propag.*, vol. 65, no. 7, pp. 3675-3683, 2017.
[25] A. P. Mohamed et al., "Simulation-Enhanced Data Augmentation for Machine Learning Pathloss Prediction," *Proc. IEEE ICC*, Denver, CO, USA, 2024, pp. 4863-4868.
[26] R. Levie, Ç. Yapar, G. Kutyniok and G. Caire, "Pathloss Prediction using Deep Learning with Applications to Cellular Optimization and Efficient D2D Link Scheduling," *Proc. IEEE ICASSP*, Barcelona, Spain, 2020, pp. 8678-8682.
[27] S. P. Sotiroudis, G. Athanasiadou, G. Tsoulos, P. Sarigiannidis, C. G. Christodoulou and S. K. Goudos, "Evolutionary Ensemble Learning Pathloss Prediction for 4G and 5G Flying Base Stations With UAVs," *IEEE Trans. Antennas Propag.*, vol. 71, no. 7, pp. 5994-6005, Jul. 2023.
[28] S. Pawar, S. Awate, M. Venkatesan, Y. Chandane, N. Rajule and Y. Anap, "Prediction of Path-loss Model for Millimeter Wave Communication using Deep Learning," *Proc. IEEE World Conf. Appl. Intell. Comput.*, Gwalior, India, 2024, pp. 642-648.
[29] R. Levie, G. Caire, and et al., "RadioUNet: Fast radio map estimation with convolutional neural networks," *IEEE Trans. Wireless Commun.*, vol. 20, pp. 4001-4015, 2021.
[30] V. V. Ratnam, H. Chen, and et al., "Fadenet: Deep learning-based mmwave large-scale channel fading prediction and its applications," *IEEE Access*, vol. 9, pp. 3278-3290, 2021.
[31] A. Ahmadi, A. Bhattacharya, M. Gratuze, S. G. Cloutier and R. A. Hadi, "UNet-Based Deep Learning Pathloss Estimator with Boundary Condition Input," *Proc. IEEE Radio Wireless Symp.*, San Juan, PR, USA, 2025, pp. 9-12.
[32] K. Qiu, S. Bakirtzis, H. Song, I. Wassell and J. Zhang, "Deep Learning-Based Path Loss Prediction for Outdoor Wireless Communication Systems," *Proc. IEEE ICASSP*, Rhodes Island, Greece, 2023, pp. 1-2.
[33] J.-H. Lee, A. F. Molisch, and et al., "PMNet: Large-scale channel prediction system for ICASSP 2023 first pathloss radio map prediction challenge," *Proc. IEEE ICASSP*, 2023.
[34] J.-H. Lee, A. F. Molisch, and et al., "PMNet: Robust pathloss map prediction via supervised learning," *Proc. IEEE Globecom*, 2023.
[35] Z. Fu, S. Mukherjee, M. T. Lanagan, P. Mitra, T. Chawla and R. M. Narayanan, "Transfer Learning and Double U-Net Empowered Wave Propagation Model in Complex Indoor Environments," *IEEE Trans. Antennas Propag.*, vol. 73, no. 7, pp. 4814-4828, Jul. 2025.
[36] REMCOM, "Wireless Insite," *https://www.remcom.com/wireless-insite-em-propagation-software*.
[37] 3GPP, "Study on channel model for frequencies from 0.5 to 100 GHz," *TR 38.901 (V15.0.0)*, Jul. 2018.
[38] L. M. Miranda Saravia, A. R. Miranda Saravia, M. M. Silva and P. V. Gonzalez Castellanos, "Prediction of Path Loss in Real-World Environments: Comparison of ITU-R P.1411 Models and Deep Learning," *Proc. IEEE Latin Amer. Conf. Antennas Propag.*, Cartagena de Indias, Colombia, 2024, pp. 1-2.
[39] M. Tercero, "5G systems: The mmMAGIC project perspective on use cases and challenges between 6-100 GHz," *Proc. IEEE WCNC Workshops*, 2016, pp. 200-205.